Research Article | Vol. 24, No. 21 | 17 Oct 2016 | OPTICS EXPRESS 23697

Optics EXPRESS

Identifying backward-rescattering photoelectron hologram with orthogonal two-color laser fields

YANG LI,[1] YUEMING ZHOU,[1,4] MINGRUI HE,[1] MIN LI,[1] AND PEIXIANG LU[1,2,3]

[1]*Wuhan National Laboratory for Optoelectronics and School of Physics, Huazhong University of Science and Technology, Wuhan 430074, China*
[2]*Laboratory of Optical Information Technology, Wuhan Institute of Technology, Wuhan 430205, China*
[3]*lupeixiang@hust.edu.cn*
[4]*zhouymhust@hust.edu.cn*

Abstract: Backscattering photoelectron hologram (BPH) originating from direct and backward-rescattering electrons encodes important structural information and ultrafast dynamics of the underlying processes. However, the BPH is usually overshadowed by other interference structures in the photoelectrons momentum spectra, preventing a direct extraction of information using BPH. Here we theoretically demonstrate disentanglement of the BPH from other types of interference with the orthogonal two-color field, where a weak orthogonal component is used to streak the BPH. By carefully adjusting the relative phase of the two-color field, the BPH is effectively separated from other interferences in the photoelectron momentum spectra and thus the BPH is unambiguously identified. This takes a significant step to time-resolved imaging of the attosecond dynamics with strong-field photoelectron holography.

OCIS codes: (320.0320) Ultrafast optics; (320.2250) Femtosecond phenomena; (320.7120) Ultrafast phenomena.

References and links

1. M. Ferray, A. L'Huillier, X. F. Li, L. A. Lompré, G. Mainfray, and C. Manus, "Multiple-harmonic conversion of 1064 nm radiation in rare gases," J. Phys. B: At. Mol. Opt. Phys. **21,** L31-L35 (1988).
2. M. Lewenstein, Ph. Balcou, M. Yu. Ivanov, A. L'Huillier, and P. B. Corkum, "Theory of high-harmonic generation by low-frequency laser fields," Phys. Rev. A **49,** 2117 (1994).
3. B. Yang, K. J. Schafer, B. Walker, K. C. Kulander, P. Agostini, and L. F. DiMauro, "Intensity-dependent scattering rings in high order above-threshold ionization," Phys. Rev. Lett. **71,** 3770 (1993).
4. G. G. Paulus, W. Nicklich, H. Xu, P. Lambropoulos, and H. Walther, "Plateau in above threshold ionization spectra," Phys. Rev. Lett. **72,** 2851 (1994).
5. H. Niikura, F. Légaré, R. Hasbani, A. D. Bandrauk, M. Yu. Ivanov, D. M. Villeneuve, and P. B. Corkum, "Sub-laser-cycle electron pulses for probing molecular dynamics," Nature (London) **417,** 917-922 (2002).
6. Y. Deng, Z. Zeng, Z. Jia, P. Komm, Y. Zheng, X. Ge, R. Li, and G. Marcus, "Ultrafast excitation of an inner-Shell electron by laser-induced electron recollision," Phys. Rev. Lett. **116,** 073901 (2016).
7. W. Becker, X. Liu, P. J. Ho, and J. H. Eberly, "Theories of photoelectron correlation in laser-driven multiple atomic ionization," Rev. Mod. Phys. **84,** 1011-1043 (2012).
8. Y. Zhou, C. Huang, Q. Liao, and P. Lu, "Classical simulations including electron correlations for sequential double ionization," Phys. Rev. Lett. **109,** 053004 (2012).
9. X. Ma, Y. Zhou, and P. Lu, "Multiple recollisions in strong-field nonsequential double ionization," Phys. Rev. A **93,** 013425 (2016).
10. A. Tong, Y. Zhou, and P. Lu, "Resolving subcycle electron emission in strong-field sequential double ionization," Opt. Express **23,** 15774-15783 (2015).
11. F. Krausz and M. Ivanov, "Attosecond physics," Rev. Mod. Phys. **81,** 163-234 (2009).
12. L.-Y. Peng, W.-C. Jiang, J.-W. Geng, W.-H. Xiong, and Q. Gong, "Tracing and controlling electronic dynamics in atoms and molecules by attosecond pulses," Phys. Rep. **575,** 1-71 (2015).
13. J. Itatani, J. Levesque, D. Zeidler, H. Niikura, H. Pépin, J. C. Kieffer, P. B. Corkum, and D. M. Villeneuve, "Tomographic imaging of molecular orbitals," Nature (London) **432,** 867-871 (2004).
14. S. Baker, J. S. Robinson, C. A. Haworth, H. Teng, R. A. Smith, C. C. Chirilă, M. Lein, J. W. G. Tisch, and J. P. Marangos, "Probing proton dynamics in molecules on an attosecond time scale," Science **312,** 424-427 (2006).
15. W. Li, X. Zhou, R. Lock, S. Patchkovskii, A. Stolow, H. C. Kapteyn, and M. M. Murnane, "Time-resolved dynamics in N2O4 probed using high harmonic generation," Science **322,** 1207-1211 (2008).

#272686 http://dx.doi.org/10.1364/OE.24.023697
Journal © 2016 Received 29 Jul 2016; revised 25 Sep 2016; accepted 26 Sep 2016; published 3 Oct 2016

Optics EXPRESS

16. O. Smirnova, Y. Mairesse, S. Patchkovskii, N. Dudovich, D. Villeneuve, P. Corkum, and M. Yu. Ivanov, "High harmonic interferometry of multi-electron dynamics in molecules," Nature (London) **460,** 972-977 (2009).
17. H. J. Wörner, J. B. Bertrand, D. V. Kartashov, P. B. Corkum, and D. M. Villeneuve, "Following a chemical reaction using high-harmonic interferometry," Nature (London) **466,** 604-607 (2010).
18. P. M. Kraus, O. I. Tolstikhin, D. Baykusheva, A. Rupenyan, J. Schneider, C. Z. Bisgaard, T. Morishita, F. Jensen, L. B. Madsen, and H. J. Wörner, "Observation of laser-induced electronic structure in oriented polyatomic molecules," Nat. Commun. **6,** 7039 (2015).
19. L. He, P. Lan, Q. Zhang, C. Zhai, F. Wang, W. Shi, and P. Lu, "Spectrally resolved spatiotemporal features of quantum paths in high-order-harmonic generation," Phys. Rev. A **92,** 043403 (2015).
20. R. Srinivasan, J. S. Feenstra, S. T. Park, S. Xu, and A. H. Zewail, "Dark structures in molecular radiationless transitions determined by ultrafast diffraction," Science **307,** 558-563 (2005).
21. T. Morishita, A.-T. Le, Z. Chen, and C. D. Lin, "Accurate retrieval of structural information from laser-induced photoelectron and high-order harmonic spectra by few-cycle laser pulses," Phys. Rev. Lett. **100,** 013903 (2008).
22. M. Meckel, D. Comtois, D. Zeidler, A. Staudte, D. Pavičić, H. C. Bandulet, H. Pépin, J. C. Kieffer, R. Dörner, D. M. Villeneuve, and P. B. Corkum, "Laser-induced electron tunneling and diffraction," Science **320,** 1478-1482 (2008).
23. C. I. Blaga, J. Xu, A. D. DiChiara, E. Sistrunk, K. Zhang, P. Agostini, T. A. Miller, L. F. DiMauro, and C. D. Lin, "Imaging ultrafast molecular dynamics with laser-induced electron diffraction," Nature (London) **483,** 194-197 (2012).
24. J. Xu, C. Blaga, K. Zhang, Y. H. Lai, C. D. Lin, T. Miller, P. Agostini and L. DiMauro, "Diffraction using laser-driven broadband electron wave packets," Nat. Commun. **5,** 4206 (2014).
25. M. Li, P. Zhang, S. Luo, Y. Zhou, Q. Zhang, P. Lan, and P. Lu, "Selective enhancement of resonant multiphoton ionization with strong laser fields," Phys. Rev. A **92,** 063404 (2015).
26. Y. Li, P. Lan, H. Xie, M. He, X. Zhu, Q. Zhang, and P. Lu, "Nonadiabatic tunnel ionization in strong circularly polarized laser fields: counterintuitive angular shifts in the photoelectron momentum distribution," Opt. Express **23,** 28801-28807 (2015).
27. X. Zhu, P. Lan, K. Liu, Y. Li, X. Liu, Q. Zhang, I. Barth, and P. Lu, "Helicity sensitive enhancement of strong-field ionization in circularly polarized laser fields," Opt. Express **24,** 4196-4209 (2016).
28. Y. Huismans, A. Rouzée, A. Gijsbertsen, J. Jungmann, A. Smolkowska, P. Logman, F. Lépine, C. Cauchy, S. Zamith, T. Marchenko, J. Bakker, G. Berden, B. Redlich, A. van der Meer, H. Muller, W. Vermin, K. Schafer, M. Spanner, M. Ivanov, O. Smirnova, D. Bauer, S. Popruzhenko, and M. Vrakking, "Time-resolved holography with photoelectrons," Science **331**, 61-64 (2011).
29. Y. Huismans, A. Gijsbertsen, A. S. Smolkowska, J. H. Jungmann, A. Rouzée, P. S. W. M. Logman, F. Lépine, C. Cauchy, S. Zamith, T. Marchenko, J. M. Bakker, G. Berden, B. Redlich, A. F. G. van der Meer, M. Yu. Ivanov, T.-M. Yan, D. Bauer, O. Smirnova, and M. J. J. Vrakking, "Scaling laws for photoelectron holography in the midinfrared wavelength regime," Phys. Rev. Lett. **109,** 013002 (2012).
30. D. Gabor, "A new microscopic principle," Nature (London) **161,** 777-778 (1948).
31. D. D. Hickstein, P. Ranitovic, S. Witte, X.Tong, Y. Huismans, P. Arpin, X. Zhou, K. Keister, C. Hogle, B. Zhang, C. Ding, P. Johnsson, N. Toshima, M. Vrakking, M. Murnane, and H. Kapteyn, "Direct visualization of laser-driven electron multiple scattering and tunneling distance in strong-field ionization," Phys. Rev. Lett. **109**, 073004 (2012).
32. M. Meckel, A. Staudte, S. Patchkovskii, D. M. Villeneuve, P. B. Corkum, R. Dörner, and M. Spanner, "Signatures of the continuum electron phase in molecular strong-field photoelectron holography," Nat. Phys. **10**, 594-600 (2014).
33. X. Bian, Y. Huismans, O. Smirnova, Kai-Jun Yuan, M. J. J. Vrakking, and A. D. Bandrauk, "Subcycle interference dynamics of time-resolved photoelectron holography with midinfrared laser pulses," Phys. Rev. A **84**, 043420 (2011).
34. X. Bian and A. D. Bandrauk, "Attosecond time-resolved imaging of molecular structure by photoelectron holography," Phys. Rev. Lett. **108,** 263003 (2012).
35. M. Li, X. Sun, X. Xie, Y. Shao, Y. Deng, C. Wu, Q. Gong, and Y. Liu, "Revealing backward rescattering photoelectron interference of molecules in strong infrared laser fields," Sci. Rep. **5,** 8519 (2015).
36. M. Haertelt, X. Bian, M. Spanner, A. Staudte, and P. B. Corkum, "Probing molecular dynamics by laser-induced backscattering holography," Phys. Rev. Lett. **116,** 133001 (2016).
37. D. B. Milošević, G. G. Paulus, D. Bauer, and W. Becker, "Above-threshold ionization by few-cycle pulses," J. Phys. B: At. Mol. Opt. Phys. **39,** R203-R262 (2006).
38. D. G. Arbó, K. L. Ishikawa, K. Schiessl, E. Persson, and J. Burgdörfer, "Diffraction at a time grating in above-threshold ionization: The influence of the Coulomb potential," Phys. Rev. A **82,** 043426 (2010).
39. X. Xie, S. Roither, D. Kartashov, E. Persson, D. G. Arbó, L. Zhang, S. Gräfe, M. S. Schöffler, J. Burgdörfer, A. Baltuška, and M. Kitzler, "Attosecond probe of valence-electron wave packets by subcycle sculpted laser fields," Phys. Rev. Lett. **108,** 193004 (2012).
40. M. Richter, M. Kunitski, M. Schöffler, T. Jahnke, L. P. H. Schmidt, M. Li, Y. Liu, and R. Dörner, "Streaking temporal double-slit interference by an orthogonal two-color laser field," Phys. Rev. Lett. **114,** 143001 (2015).
41. M. He, Y. Li, Y. Zhou, M. Li, and P. Lu, "Temporal and spatial manipulation of the recolliding wave packet in strong-field photoelectron holography," Phys. Rev. A **93,** 033406 (2016).
42. D. B. Milošević, "Forward- and backward-scattering quantum orbits in above-threshold ionization," Phys. Rev. A **90,** 063414 (2014).

Optics EXPRESS

43. D. B. Milošević, "Low-frequency approximation for above-threshold ionization by a laser pulse: low-energy forward rescattering," Phys. Rev. A **90,** 063423 (2014).
44. C. Figueira de Morisson Faria, H. Schomerus, and W. Becker, "High-order above-threshold ionization: The uniform approximation and the effect of the binding potential," Phys. Rev. A **66,** 043413 (2002).
45. E. Hasović, W. Becker, and D. B. Milošević, "Electron rescattering in a bicircular laser field," Opt. Express **24,** 6413-6424 (2016).
46. D. B. Milošević and W. Becker, "Improved strong-field approximation and quantum-orbit theory: application to ionization by a bicircular laser field," Phys. Rev. A **93,** 063418 (2016).
47. L. Tao and A. Scrinzi, "Photo-electron momentum spectra from minimal volumes: the time-dependent surface flux method," New J. Phys. **14,** 013021 (2012).
48. D. Bauer and P. Koval, "QPROP: A Schrödinger-solver for intense laser-atom interaction," Comput. Phys. Commun. **174,** 396-421 (2006).
49. V. Mosert and D. Bauer, "Photoelectron spectra with Qprop and t-SURFF," Comput. Phys. Commun. **174,** 452-463 (2016).
50. Y. Zhou, O. I. Tolstikhin, and T. Morishita, "Near-forward rescattering photoelectron holography in strong-field ionization: extraction of the phase of the scattering amplitude," Phys. Rev. Lett. **116,** 173001 (2016).
51. O. I. Tolstikhin and T. Morishita, "Adiabatic theory of ionization by intense laser pulses: Finite-range potentials," Phys. Rev. A **86,** 043417 (2012).
52. A. Čerkić, E. Hasović, D. B. Milošević, and W. Becker, "High-order above-threshold ionization beyond the first-order Born approximation," Phys. Rev. A **79,** 033413 (2009).
53. X. Bian and A. D. Bandrauk, "Orientation-dependent forward-backward photoelectron holography from asymmetric molecules," Phys. Rev. A **89,** 033423 (2014).

1. Introduction

When an atom or molecule is exposed to a strong laser field, an electron wave packet can be ionized through tunneling. The ionized electron wave packet may be driven back to parent ion, result in various phenomena such as high harmonic generation [1, 2], elastic scattering [3, 4], inner-shell electron exciation [5, 6] and nonsequential double ionization [7–10]. The laser-induced rescattering or recombination accesses the richness of electronic structural and dynamical information of the target [11, 12]. Many approaches relied on the laser-driven electron rescattering have been proposed to follow the electron dynamics and detect target structures in a time-resolved manner, such as high-harmonic spectroscopy [13–19], photoionization and photoelectron spectroscopy [20–27]. Among them, one fascinating way is strong field photoelectron holography [28, 29].

By analogy to the conventional optical holography [30], the strong field holography is recognized as the interference of tunneling electron wave packets drifting directly to the detector (reference wave) and those undergoing rescattering by the parent ion (signal wave). The first experimental demonstration of strong field holography was performed by Huismans *et al*, where a "spider-like" interference structure was identified in photoelectron momentum distribution (PMD) of xenon [28] and then observed for other atoms [31] and molecules [32]. Theoretical analysis has shown that the spider-like structure is a kind of forward-scattering photoelectron hologram (FPH) [28, 33]. It is the near-forward rescattering electrons that record the structure information of the target. For this near-forward rescattering process, the electrons do not catch much information about the core because of the very soft recollision with the core. In order to gain more information of the target, one can use the hologram from the direct and backward-rescattering electrons, i.e., the backscattering photoelectron hologram (BPH) [34]. However, the BPH is usually very difficult to be identified in the experiment. The reasons come from two folds. Firstly, in linearly-polarized laser fields, a train of several electron wave packets released at different ionization times can interfere with each other within one pulse. One kind of interference is convoluted and overlapped with several other interference events. The intracycle interference pattern between direct electrons liberated from adjacent quarter cycles of the laser pulse has a very similar structure with BPH. Both the number and width of the interference stripes as well as the spacing between the stripes are similar. So it is very hard to distinguish the BPH from the intracycle interference [33, 35]. Secondly, due to the small scattering cross sections of atoms,

Optics EXPRESS

the signal of backward-rescattering electrons is very weak and the BPH is nearly impossible to be resolved in the PMD. Recently, Haertelt *et al* experimentally measured the BPH using differential holography technique for H_2 with different alignments [36]. However, how to determine BPH and directly observe it remain to be great challenges.

In this paper, we propose a method to identify BPH using an orthogonal two-color (OTC) control scheme. By introducing a weak orthogonal streaking laser field at long wavelength, i.e., in mid-infrared region, we show that the multiple tunneling electron wave packets as well as the recollision process of the returning electron wave packets can be precisely controlled by tuning the relatively phase of the two frequency components. At some relative phases, the signal of backscattering electrons is comparable with that of the direct electrons, providing favorable conditions for observing BPH. At the same time, the intracycle interference is suppressed and it is streaked to different areas with BPH in the PMD. Thus the BPH can be unambiguously revealed. Our results are confirmed by numerical solutions of the corresponding full-dimensional time-dependent Schrödinger equation (TDSE), suggesting a promising way in studying structural information and dynamic processes using photoelectron holography.

2. Results and discussions

Firstly, we illustrate the obstacles that prevent us from observing the BPH in a linearly-polarized laser pulse in detail within the framework of the strong-field approximation (SFA) model [2, 37]. Figures 1(a) and 1(b) show the intracycle interference pattern between direct electrons [38–40]. The formation of this intracycle interference can be understood as follows: it arises from two electron wave packets liberated at adjacent half cycles, where the electric fields have opposite values (see the upper row) while the vector potentials are the same. As shown in the middle row, the two electron wave packets firstly tunnel from the opposite side of the parent ion and finally achieve the same drift momentum. One electron wave packet goes directly to the detector and the other reverses its motion and goes across the core without being rescattered. The induced intracycle interference pattern manifest itself as a set of incoming semirings (i.e., with a rightward curvature) in the positive momentum region ($p_x > 0$) as displayed in the bottom panel of Fig. 1(b). Note that we present here the interference pattern between electrons ionized at [0T, 0.5T] and [0.5T, 1T]. Actually, electrons released at [0.5T, 1T] and [1T, 1.5T] can also interfere. The shape of the interference pattern is the same, but with an opposite curvature. Figures 1(c) and 1(d) present the FPH and BPH, respectively. The FPH originates from electrons ionized at adjacent quarter cycles. The electron released at the falling edge of the electric field serves as the signal wave, marked as A in Fig. 1(c). It moves across the core and is rescattered forward, and then interferes with the reference wave marked as B. This kind of FPH is a set of outgoing semirings in the negative momentum region ($p_x < 0$). We would like to point out that the FPH presented here is another kind of FPH with different ionization times for signal and reference electrons, which is different from the spider-like hologram (not shown). Similarly, the BPH arises from electrons ionized at instants with a quarter-cycle interval, shown in Fig. 1(d). The signal electron (marked as A) is backscattered, interfering with reference electron which goes across the core without being rescattered. The BPH appears in the positive momentum space as incoming fringes. Comparing with Fig. 1(b), it is easy to find that the BPH is very similar with intracycle interference. The fringes have the same curvature; the number and shape of the fringes are similar; the width of the fringes as well as the space between them increases as the increase of the parallel momentum p_x. So it is not easy to distinguish the BPH from intracycle interference in PMD using linearly-polarized laser fields. Moreover, the signal of backward-rescattering electrons is much weaker than the interfering direct electrons, making the BPH have a very low contrast and nearly invisible in PMD. Thus even if one observes semiring structures similar as BPH in PMD, it is most likely the intracycle interference rather than the BPH.

Optics EXPRESS

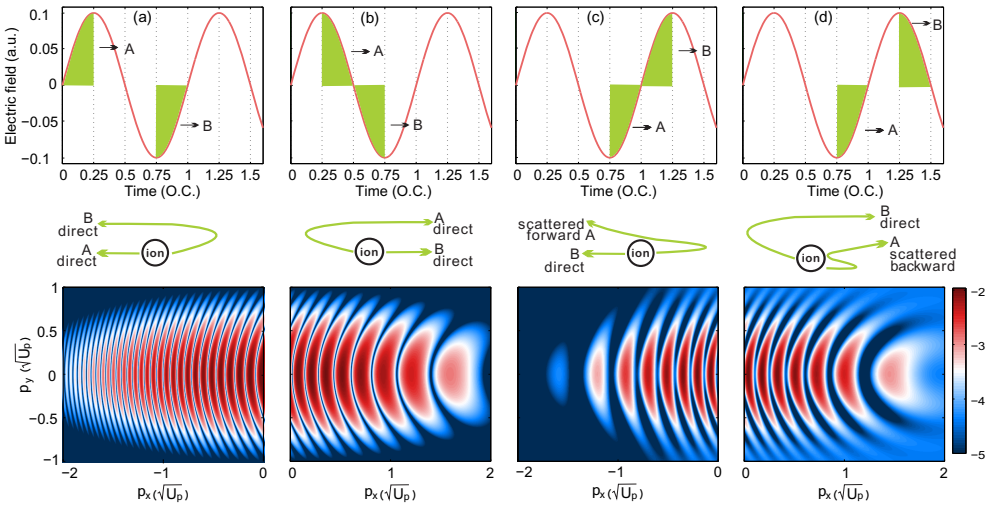

Fig. 1. Illustration of different photoelectron interferences in linearly-polarized laser fields, calculated by SFA. (a) and (b) The intracycle interferences between direct electrons. (c) The forward-scattering photoelectron hologram. (d) The backscattering hologram. The upper row shows the ionization times of the involved interfering electron wave packets A and B. The middle row presents the sketch of the corresponding electron trajectories. The calculated interference fringes are displayed in the bottom row. The laser intensity is 3.0×10^{14}W/cm^2 with a wavelength of 800 nm.

In the following, we analyze the changes of intracycle interference and hologram in orthogonal two-color laser fields. The OTC fields are composed of an 800-nm fundamental field polarized along x direction with intensity of 1.0×10^{14}W/cm^2 and a weaker 1600-nm field polarized along y direction with intensity of 2.5×10^{13}W/cm^2. The time-dependent electric field $\mathbf{E}(t)$ of the OTC fields is defined as

$$\mathbf{E}(t) = f(t)[E_x \cos(\omega t)\mathbf{e}_x + E_y \cos(\omega t/2 + \phi)\mathbf{e}_y]. \tag{1}$$

Here, $f(t)$ is the pulse envelope which has a $\sin^2(\pi t/\tau)$ form. The total duration τ is $8T$ (T is the optical cycle of the 800-nm pulse). $\omega = 0.057$ a.u. is the angular frequency of the 800-nm pulse and ϕ is the relative phase between the two components. Since the 1600-nm field is relatively weak, the tunneling of the electron wave packets is mainly induced by the 800-nm field. The 1600-nm pulse only streaks the electron in the orthogonal direction. We use the generalized SFA model to analyze the holograms and other interference patterns in OTC fields [41]. This is done by the application of saddle-point method to the standard S-matrix expressions in the SFA [42, 43]. The corresponding transition amplitudes of direct and rescattering electrons are expressed as

$$M_{\mathbf{p}}^{d} = -i \sum_{s} \sqrt{\frac{2\pi i}{S_i''(t_{is})}} \langle \mathbf{p} + \mathbf{A}(t_{is}) | \mathbf{r} \cdot \mathbf{E}(t_{is}) | \Psi_0 \rangle \exp[iS_i(t_{is})] \tag{2}$$

and

$$\begin{aligned} M_{\mathbf{p}}^{r} = & -\sum_{s} \sqrt{\frac{(2\pi i)^5}{\det(\partial^2 S_r/\partial q_j \partial q_k)_{j,k=1,2,\ldots 5}}} \\ & \times \langle \mathbf{p} + \mathbf{A}(t_{rs}) | V(r) | \mathbf{k}_s + \mathbf{A}(t_{rs}) \rangle \\ & \times \langle \mathbf{k}_s + \mathbf{A}(t'_{is}) | \mathbf{r} \cdot \mathbf{E}(t'_{is}) | \Psi_0 \rangle \exp[iS_r(\mathbf{k}_s; t'_{is}, t_{rs})], \end{aligned} \tag{3}$$

Optics EXPRESS

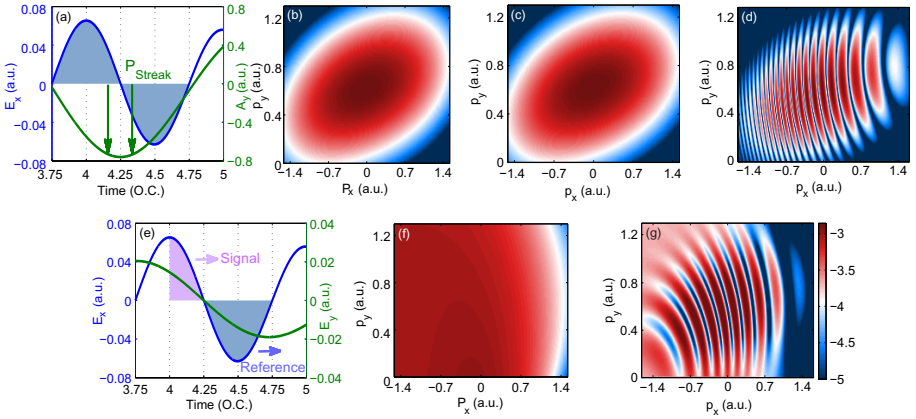

Fig. 2. Different photoelectron interferences in orthogonally polarized two-color laser fields with relative phase of 0.25π calculated by SFA. (a) The vector potential (green curve) of the 1600-nm streaking field relative to the 800-nm fundamental electron field (blue curve). Here they are drawn in parallel for better visualization of the streaking dynamics. The light blue shading areas indicate the ionization times of the two direct electron wave packets. Green arrows show the momentum streaking of electrons by 1600-nm field. (b) and (c) The momentum distributions of direct electrons ionized at the two shading areas in (a), respectively. (d) The intracycle interference structure of direct electrons. (e) The electric field of 800-nm (blue curve) and 1600-nm (green curve) laser fields, respectively, drawn in parallel as well. The pink shading area shows the ionization times of signal electrons and the light blue area shows the ionization times of reference electrons. (f) The momentum distribution of signal electrons. (g) The forward- (positive momentum region) and backward- (negative momentum region) rescattering holograms. Intensities of the 800-nm and 1600-nm fields are $1 \times 10^{14}\mathrm{W/cm^2}$ and $2.5 \times 10^{13}\mathrm{W/cm^2}$, respectively. Other parameters are given in the main text.

respectively. In the above equations, Ψ_0 is the initial wave function. $\mathbf{A}(t) = -\int_0^t dt'\mathbf{E}(t')$ is the vector potential of the OTC fields. $\mathbf{p}$ is the final asymptotic momentum. t_{is} is the ionization time of direct electrons. t'_{is}, t_{rs} and $\mathbf{k}_s$ are the ionization time, rescattering time and the drift momentum of rescattering electrons. S_i and S_r are the semiclassical actions of direct and rescattering electrons. q_j $(j = 1, 2, \ldots 5)$ runs over t'_{is}, t_{rs} and the three components of $\mathbf{k}_s$. The explicit form of Eq. (3) depends on the potential $V(r)$. For backscattering electrons, the Coulomb form of the potential will lead to the well-known divergence [44]. However, this does not affect the shape of the electron spectra. Here, we focus on the interference of the electron wave packet, which is mainly determined by the exponential terms of the transition amplitudes. Thus the pre-exponential terms is omitted for simplicity.

Figure 2(a) shows electric field of the 800-nm pulse (blue curve) and the vector potential of the 1600-nm pulse (green curve) for the relative phase $\phi = 0.25\pi$. We take the interference of two electron wave packets ionized within [3.75T, 4.25T] and [4.25T, 4.75T] as the example. For $\phi = 0.25\pi$, these two electron wave packets experience the same vector potential of the 1600-nm pulse, as indicated by the green arrows. In this case, the momentum distributions of these direct electrons are identical, as presented in Figs. 2(b) and 2(c). As a result, they are indistinguishable in the final momentum distribution, satisfying the interference conditions. Since these two electron wave packets are ionized in the same optical cycle, the interference between them is the intracycle interference, as exhibited in Fig. 2(d). One can find that the intracycle interference pattern is only streaked in the y direction, with an overall shape similar with that in the linearly-polarized field. It is worth mentioning that different from the case of

Optics EXPRESS

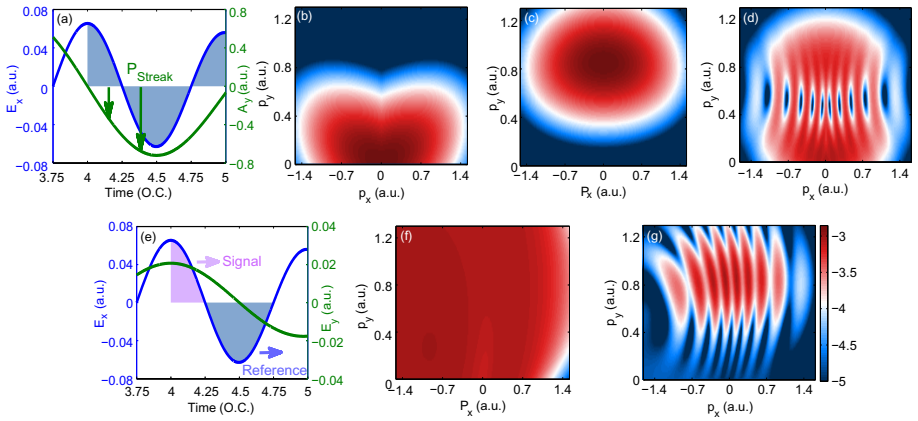

Fig. 3. Same as Fig. 2 but for relative phase of $\phi = 0$.

linearly-polarized field, electrons ionized within [4.25T, 4.75T] and [4.75T, 5.25T] experience opposite vector potentials of the 1600-nm pulse. Thus the intracycle interference between these two electron wave packets is switched off.

Next we turn to holographic interference for the case of $\phi = 0.25\pi$. Signal electrons ionized at [4.0T, 4.25T] and reference electrons ionized at [4.25T, 4.75T] are considered, as displayed in Fig. 2(e). Figure 2(f) shows the momentum distribution of signal (rescaterring) electrons. It should be mentioned that the number of rescattering quantum orbits is increased in a two-dimensional laser field [45]. These quantum orbits are well classified and clearly analyzed in [46]. Here since the intensity of the 1600-nm orthogonal component is much lower than that of the main 800-nm component, we only consider one main rescattering quantum orbit at [4.0T, 4.25T]. The resulting holographic interference pattern with reference electron is shown in Fig. 2(g). The interference fringes in the positive momentum space ($p_x > 0$) are FPH, and those in the negative momentum space ($p_x < 0$) are BPH. Due to the streaking of 1600-nm pulse, the hologram is also streaked in the transverse direction. Thus in the final momentum-resolved electron spectra, the BPH are still overlapped with the intracycle interference. However, compared with intracycle interference structure in Fig. 2(d), the curvature of the BPH fringes is left-downward, which is opposite to that of intracycle interference fringes. Therefore the BPH and intracycle interference become distinguishable.

Although the BPH can be distinguished from intracycle interference for $\phi = 0.25\pi$, they are overlapped with each other, and because the signal of backscattering electrons is very weak, it is still difficult to identify BPH with good resolution. Below we change the relative phase of the OTC laser fields to 0 and analyze the change of interference patterns. Figure 3(a) shows electric field of the 800-nm pulse (blue curve) and the vector potential of the 1600-nm pulse (green curve) for the relative phase $\phi = 0$. The intracycle interference of two electron wave packets ionized within [4.0T, 4.25T] and [4.25T, 4.5T] is considered. Figures 3(b) and 3(d) display the momentum distributions of these direct electrons, respectively. One can see that they are mostly separated in the momentum space. Electrons ionized within [4.0T, 4.25T] reach the momentum space of $p_y \in [0.5, 1.2]$ a.u., while the final momenta of electrons ionized in [3.75T, 4T] are in the momentum space of $p_y \in [0, 0.5]$ a.u. The reason is that these two electron wave packets experience different vector potentials of the 1600-nm field for $\phi = 0$. The 1600-nm field streaks electrons released in [4.25T, 4.5T] to a larger transverse momentum than those ionized in [4.0T, 4.25T], as indicated by the green arrows in Fig. 3(a). Only in the region around $t = 4.25$T are the vector potentials close. Thus considering the initial transverse momentum distribution, only electrons tunnel around $t = 4.25$T can overlap in momentum space and interfere

Optics EXPRESS

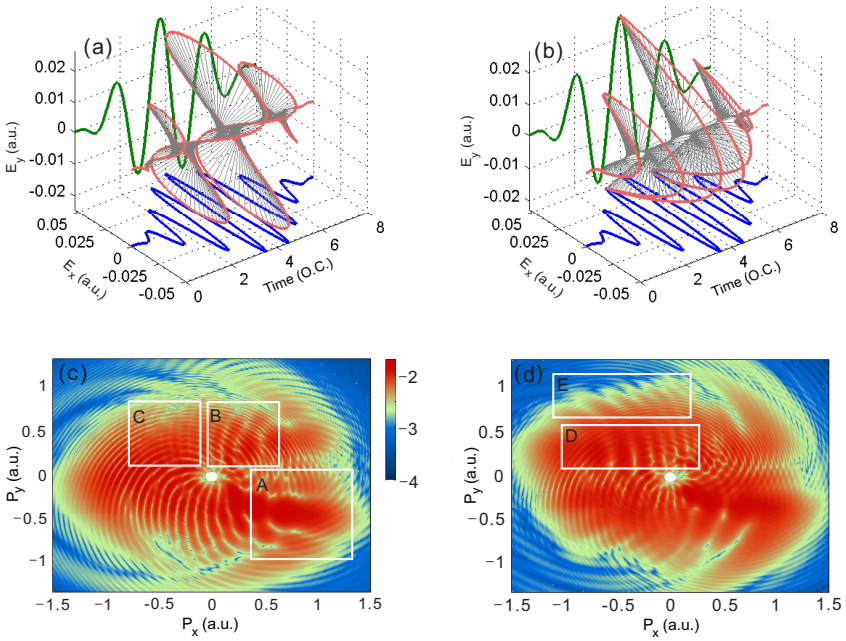

Fig. 4. The electric fields (red curves) of the OTC pulses for relative phases of (a) $\phi = 0.25\pi$ and (b) $\phi = 0$. The OTC fields are composed of an 800-nm fundamental field polarized along x direction with intensity of 1.0×10^{14}W/cm^2 and a weaker 1600-nm field polarized along y direction with intensity of 2.5×10^{13}W/cm^2. The two components are displayed by blue and green curves, respectively. The total duration is 8 optical cycles of the 800-nm pulse. (c) and (d) The 2D PMDs calculated by solving TDSE for $\phi = 0.25\pi$ and $\phi = 0$, respectively. The squared regions marked by A-E indicate different types of interference structures.

with each other. The intracycle interference is presented in Fig. 3(d). One can clearly find that electrons with momenta around $p_y = 0.5$ a.u. are overlapped. Thus the intracycle interference only appears around in this momentum region, and it is highly suppressed.

Next we focus on the change of BPH for the case of $\phi = 0$. Still signal electrons ionized at $[4.0\text{T}, 4.25\text{T}]$ and reference electrons ionized at $[4.25\text{T}, 4.75\text{T}]$ are considered, as indicated in Fig. 3(e). In comparison with Fig. 2(e), the signal electrons experience different force of the 1600-nm field, as shown by the green curve. Thus the signal electrons, especially the backscattering electrons, change the momentum, leading to different momentum distributions of the final states, as shown in Fig. 3(f). In this way, the hologram exhibits different features shown in Fig. 3(g). Again the interference fringes in the positive momentum space ($p_x > 0$) are FPH, and those in the negative momentum space ($p_x < 0$) are BPH. The main feature of the hologram is the fringes mostly distribute in the region $p_y \in [0.5, 1.2]$ a.u., where the intracycle interference is nearly switched off, result in the separation of the BPH and intracycle interference in final momentum-resolved electron spectra. based on above findings, we show that using the OTC field with relative phase $\phi = 0$ is an very effective way to identify BPH based on the results of SFA.

In order to confirm the prediction of SFA results, we explicitly solve the full-dimensional TDSE for hydrogen using the t-SURFF method [47–49]. The t-SURFF method combines exact numerical solutions in an inner region with approximate analytical Volkov solutions in the outer region. The boundary of the inner region is $r_{max} = 100$ a.u. and the maximum angular momentum is $L_{max} = 100$. The step size of the radial grid is chosen as $\delta r = 0.2$ a.u. and

Optics EXPRESS

the time step is $\delta t = 0.0375$ a.u. Convergence is checked by varying the radial grid step δr down to 0.1 a.u. and time step δt down to 0.01 a.u. Laser parameters are the same as in SFA calculations. In Figs. 4(a) and 4(b), we present the real OTC fields (red curves) together with the two components (blue and green curves) for $\phi = 0.25\pi$ and $\phi = 0$, respectively. This may help the readers to get an intuitive impression of what the OTC fields look like for different relative phases. The 2D PMDs in the polarization plane obtained from the TDSE calculations for different relative phases are displayed in Figs. 4(c) and 4(d), respectively. Figure 4(c) exhibits the PMD for $\phi = 0.25\pi$. There are rich interference structures in the PMD. In general, three interference stripes can be identified, as marked by A, B and C. The interference stripes in region A are the general spider-like FPH induced by signal and reference electrons ionized within the same quarter cycle. The second interference pattern in region B is the intracycle interference manifesting itself as nearly vertical stripes. Note that the intracycle interference appears in both the first and second quadrants of the PMD. In region B we only show a few obvious stripes. The third one in region C is the BPH, which is aimed to be identified. As can be seen, the most conspicuous interference pattern in region C is still the intracycle interference. Comparing with Fig. 2(g), the BPH pattern is so weak that nearly impossible to be resolved. The reason is that the BPH and the intracycle interference are overlapped for the case of $\phi = 0.25\pi$. Although the structure of BPH is different from the intracycle interference, the signal of rescattering electron is too weak in comparison with direct electrons, making the BPH hard to be resolved in the PMD. This point is also predicted by the SFA calculations. In Fig. 4(d), the PMD obtained from TDSE calculations with relative phase of $\phi = 0$ is shown. In region E of $p_y \in [0.5, 1.2]$ a.u. marked by white box, it can be seen that the BPH structure is very well revealed, in consistent with the SFA results in Fig. 3(g). In comparison, the intracycle interference, manifesting itself as nearly vertical fringes, is localized in region D of $p_y < 0.5$ a.u. While it is nearly invisible in region E where the BPH dominates. This also confirms that the BPH and intracycle interference are separated for $\phi = 0$. The second reason why the BPH is well resolved in high transverse momentum region can be attributed to the fact that the ionization probability of electrons obeys a Gaussian distribution with respect to the initial transverse momentum. In large transverse momentum region where the BPH appears, the ionization probability of reference electron is relatively low. So the signals of backscattering and direct electrons become comparable, providing another advantage to observe the BPH. Therefore, the BPH is clearly identified for the case of $\phi = 0$.

During laser-induced electron scattering process, the long-range Coulomb potential dominates and contributes most to cross sections of forward scattering electrons, thus the short-range detailed atomic and molecular structures are barely reflected in FPH. In contrast, the BPH is more sensitive to the short-range effects and thus records more structural information. In a linearly-polarized laser field, the backscattering hologram is usually buried below other orders-of-magnitude more intense channels such as FPH and intracycle interference. Using a weak streaking field at long wavelength and tuning the relative phase, we successfully reveal the backscattering hologram in the PMD, as presented in Fig. 4(d). Theory of extracting structural information of atoms and molecules from FPH is recently established in [50], and can be directly extended to analyze the backscattering hologram in the present case. In addition, the signal and reference waves are born from different quarter cycles. Using the SFA model, the birth time of backscattering holographic fringes can be precisely determined within dozens of attoseconds. Thus the BPH can probe attosecond dynamical electronic process.

Before closing, we would like to add a few remarks about the concept of strong-field photoelectron holography. The term “holography” with respect to the interference of direct and rescattering electrons was first introduced in [28]. The so-called holographic pattern observed in [28] has already attracted much interest as a new promising means to provide time-resolved imaging of ultrafast processes. In the recently developed adiabatic theory [51], the ionization

amplitude can be separated into adiabatic (direct) and rescattering parts. These two parts appear in the different orders of the adiabatic parameter, and hence are well defined and well separated. Note that this is a rigorous statement as proved in [51]. In the strong-field photoelectron holography, the adiabatic and rescattering parts of the ionization amplitude act as the reference and signal waves in optical holography, respectively. It is shown in [50] that the signal wave bears structure information, i.e., the phase of the scattering amplitude, while the reference wave does not. Thus the PMD can be viewed as a kind of hologram encoding the structural information. Theoretical procedure has been developed to extract this structure information [50] from FPH. An alternative way to extract the phase of scattering amplitude has been introduced in [52], using the low-frequency approximation. This is done by rewriting the rescattering amplitude beyond the first Born approximation, i.e., by replacing the outgoing plane wave with the exact scattering wave in Eq. (3). The purpose of the present paper is identifying BPH, which is much harder than observing FPH. Extracting the phase of the scattering amplitude from the hologram using a more delicate theory beyond the first Born approximation is the goal of our future research.

3. Conclusion

In summary, we present a novel approach to reveal backscattering photoelectron hologram using OTC fields. The weak streaking field at long wavelength acts as an electron steerer, which effectively separates different interferogram in both temporal and spatial domains. As a result, the previously unobserved BPH is unambiguously identified in PMD. The BPH not only provides deep insight into the subcycle dynamics in the strong-field ionization process [36], but also serves as a sensitive probe of the target structure [34, 50, 53]. Our results have demonstrated the ability of disentangling the interference structures and revealing BPH with sculpturing laser pulse, which will benefit time-resolved imaging of the ultrafast dynamics with photoelectron interferometry.

Funding

National Natural Science Foundation of China (NNSFC) (61405064, 11234004, 61475055) and China Postdoctoral Science Foundation (CPSF) (0106012026).

Acknowledgment

Numerical simulations presented in this paper were carried out using the High Performance Computing Center experimental testbed in SCTS/CGCL (see http://grid.hust.edu.cn/hpcc).